Thermal and Mechanical Behavior of Copper Molds during Thin-Slab Casting (I): Plant Trial and Mathematical Modeling

JOONG KIL PARK, BRIAN G. THOMAS, INDIRA V. SAMARASEKERA, and U. SOK YOON

Three-dimensional (3-D) finite-element thermal-stress models have been developed to predict temperature, distortion, and residual stress in the mold of continuous casters of thin steel slabs, comparing both funnel-shaped and parallel molds. The mold shape and high casting speed leads to higher mold temperatures and shorter mold life than in conventional slab casters. This study investigates heat flux and the effects of mold shape on distortion and cracking of the thin-slab mold. In Part I of this two-part article, mold wall temperatures measured in the plant were analyzed to determine the corresponding heat-flux profiles in thin-slab molds. This data was then used in an elastic-visco-plastic analysis to investigate the deformation of the molds in service for the two different mold shapes. The model predictions of temperature and distortion during operation match plant observations. During operation, the hot-face temperature reaches 580 °C and heat flux varies from 7 to 4.5 MW/m^2 when casting at 3.6 m/min. The copper plates bend toward the steel, with a maximum outward distortion of about 0.3 mm. This occurs just above the center of the wide faces and is smaller than the distortion of a conventional slab mold.

I. BACKGROUND

AN important recent trend in the steel industry is the development of processes for casting steel closer to the final product size. The continuous casting of thin slabs with only a few centimeters of thickness allows hot-direct rolling to be performed inline with a conventional finishing mill, eliminating the need for a roughing train. This advanced continuous-casting technology of thin slabs is growing in the steel industry owing to the associated savings in capital cost, energy, and manpower.

The mold is the most critical component of the process, which controls initial solidification and determines surface quality. The quantification of heat transfer and distortion of thin-slab casting, copper mold plates has received relatively little attention in previous literature. Furthermore, the difference between the funnel and parallel mold design has not been compared.

During operation, the mold distorts due to the steep thermal gradients. Although this distortion is very small, it may affect the size of the gap between the solidified shell and the mold, which, in turn, controls heat transfer. Thin-slab molds are expected to have higher heat flux and temperature owing to the higher casting speed. The accompanying thermal stress may cause permanent creep deformation near the meniscus, which affects mold life as well. Furthermore, maintaining a reliable, crack-free mold within close dimensional tolerances is also crucial to safety and productivity.

JOONG KIL PARK, Graduate Student, and INDIRA V. SAMARASEKERA, Professor, are with the Department of Metals and Metallurgical Engineering, University of British Columbia, Vancouver, BC, Canada V6T 1Z4. Contact e-mail: vpr@exchange.ubc.ca BRIAN G. THOMAS, Professor, is with the Department of Mechanical and Industrial Engineering, University of Illinois at Urbana-Champaign, Urbana, IL 61801. U.-SOK YOON, Senior Researcher, is with the Iron & Steelmaking Research Group, Technical Research Laboratory, POSCO, Pohang, Kyungbuk, Korea.

Manuscript submitted May 29, 2001.

This article is the first part of a two-part study on the thermal and mechanical behavior of thin-slab casting molds. This part investigates the heat-flux profiles based on mold temperature measurements and compares the thermal distortion of thin-slab molds of two different configurations using three-dimensional (3-D) finite-element models.

II. PREVIOUS WORK

Many mathematical models and plant trials have investigated the thermal and mechanical behavior of conventional slab-casting molds.[1–7] Thomas *et al.*[1,2] applied a 3-D elastic-plastic-creep finite-element model to predict temperature and distortion of a conventional slab mold during operation. The wide faces were predicted to bend inward (toward the steel) with a maximum distortion on the order of 1 mm on the wide-face centerline between the meniscus and mold midheight. They also studied the effect of design and operating variables, such as slot spacing and shape, copper plate thickness, strand width, clamping force, ferrostatic pressure, pretension stress, water-box thickness, and copper alloy. Several ways were suggested to reduce detrimental residual stress and strain, such as designing water slots to lower hot-face temperature and optimizing the clamping force.

Tada *et al.*[3] studied the factors affecting the performance and service life of continuous-casting slab molds. They emphasized that optimization of the design and maintenance of the cooling-water delivery system should improve uniformity of heat transfer, with resulting improvements in mold life and reduction in sticking corner breakouts.

Ozgu[4] instrumented a slab mold to measure a wide range of operating parameters, including mold wall temperature and deformation. He found that although the fixed and loose sides of the mold deformed by different amounts, both deformed shapes were convex toward the mold cavity during steady-state operation, and the mold cavity decreased by

0.96 mm in the middle of the mold and increased by about 2 mm at the ends of the mold. The measured distortion behavior was consistent with the predictions of Thomas.[2]

Salkiewicz and Ratka[5] measured the effect of copper alloy properties on permanent distortion and wear of copper mold plates. They measured very large width contractions (1.02 to 8.38 mm) of the mold plates, with a convex-downward shape across the top and bottom of the plates.

Hashimoto *et al.*[6] have analyzed temperature, distortion, and thermal stress in a fully constrained, slab mold plate including creep, and predicted a permanent 0.2 to 0.3 mm contraction of the wide face after repeated thermal cycling, depending on the copper properties. They found that thinner mold plates have lower temperatures and reduced thermal stresses, resulting in less mold plate distortion. They also observed that to prevent permanent distortion of the mold plate it should be allowed to move relative to the water cooling box.

O'Connor and Dantzig[7] developed an elastic-plastic-creep finite-element model of a funnel mold. The two-dimensional model predicted 1.75 pct of cyclic inelastic strain in a region below the meniscus along the funnel edge, which resulted from the combination of locally high temperatures coupled with geometric restraint of the mold. Based on this, they calculated locations and time to crack failure of the mold using a fatigue model.

Relatively little effort has been invested to understand the mechanical behavior of thin-slab molds, which have higher casting speed (3.5 to 5 m/min) compared to the conventional slab-casting process (usually 1 to 2.5 m/min). Further work is needed to quantify thin-slab mold temperature and distortion behavior with measurements, to apply fully 3-D mechanical models to understand crack formation, and to compare the relative merits of different mold designs. These are the aims of the current work.

III. PLANT TRIALS

A. *Mold Temperature Measurement*

A plant trial was conducted with an instrumented parallel mold at POSCO Kwangyang works in South Korea, casting a 1260 × 70 mm thin slab at 3.6 m/min. The mold was Cu-0.1 pct Cr-0.15 pct Zr and 1000-mm long; other relevant details are given in Table I. In this table, the effective wall thickness is defined as the minimum distance from the water channel to the hot face and was relatively constant on each face. It is noted that to prevent the mold temperature from increasing to high temperatures near the meniscus, extra angled water slots were added. Figure 1 shows the backside view of the parallel mold for the plant trial, where the mold was instrumented with seven rows of K-type (chromel/alumel) thermocouples along the centerline of the mold for both the loose and fixed broad faces. Each broad face has seven columns of thermocouples for at least the first two rows. Each thermocouple was inserted through a hole drilled along the center of a tension bolt. When the tension bolts were tightened, a spring pushes the thermocouple to the required depth of 22 mm from the hot face. A copper washer was also employed at the tip of each tension bolt in order to prevent water from penetrating to the tip of the thermocouple. An electromagnetic brake system (EMBR), installed in the mold to control fluid flow, generated electromagnetic forces during mold oscillation, which caused electrical noise in the temperature data. To avoid this effect, the bare portion of the parallel thermocouple wires were held slightly apart against the mold surface in order to include a small portion of the copper mold in the thermocouple circuit.

Table I. Conditions for Plant Trial Measurements of Mold Temperature, *etc.*

	Parallel Mold	Funnel Mold
Mold coppers	Cu-0.5wt% Cr-0.1wt% Zr	
Slab thickness (mm)	75	
Slab width (mm)	1260	1140
Steel grade (carbon content, wt pct)	0.04	
Mold powder		
Basicity	1.32	
Viscosity at 1300 °C (poise)	0.52	
Meniscus level (mm)	100	
Copper plate thickness (wide face) (mm)	60	60 to 85
Effective wall thickness (mm)		
Wide face	25	25 to 27
Narrow face	22	
Mold coating material (thickness)	Cr (0.01 mm)	
Cooling water velocity (m/s)		
Wide face	10.7	10.5
Narrow face	10.6	
Water flow rate (L/min)		
Wide face	4330	4600
Narrow face	250	
Cooling water temperature (°C)		
Inlet	37.8	39.7
Outlet	48.1	47.5
Casting speed (m/min)	3.6	4.2
Number of thermocouples (EA)	42 (Fig. 1)	7

The accuracy of the temperature measurement system was assessed by an independent laboratory test. A small, scrapped copper plate was instrumented with thermocouples as described previously. The plate was immersed in boiling water, and the measured temperatures were within 1 °C of 100 °C. A second test, on the assembled instrumented mold, found the thermocouple readings between heats to match the mold water temperature.

Temperatures were also measured in a funnel mold using similar thermocouples just at the meniscus. Attention was focused on the row of seven thermocouples near the meniscus, 100 mm below the top of the loose face of the mold. This was used to investigate the temperature profile and thermal fluctuation in the mold and its effect on mold crack occurrence presented in Part II.

B. *Other Measurements*

During the plant trial, various other process parameters, such as the casting speed, the metal-level signal (cobalt source method), the temperature, and the flow rate of the cooling water were collected directly from the plant control system once per second during casting. Figure 2 compares the metal-level and casting-speed signals during steady-state casting for the parallel and funnel mold. The fluctuations are stable within a maximum ±4 mm. It seems that the funnel mold has a lower fluctuation frequency of about 0.05

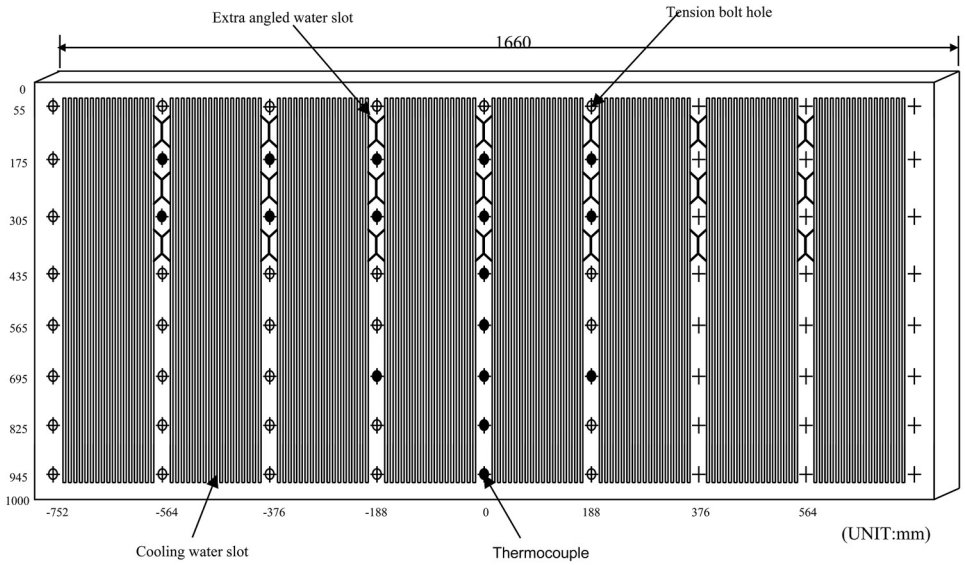

Fig. 1—Back view of the broad face of the parallel mold showing slot geometry and thermocouple locations in bolt holes (solid circle).

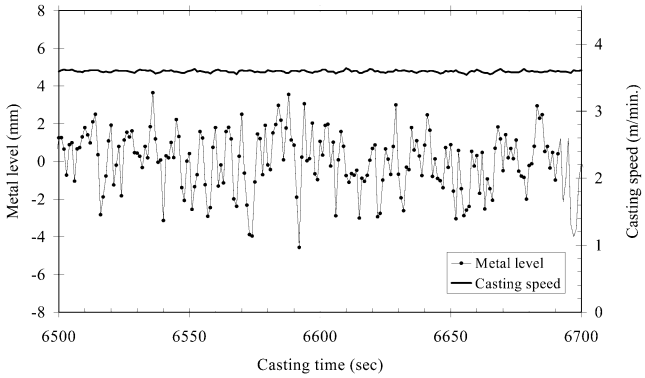

(*a*)

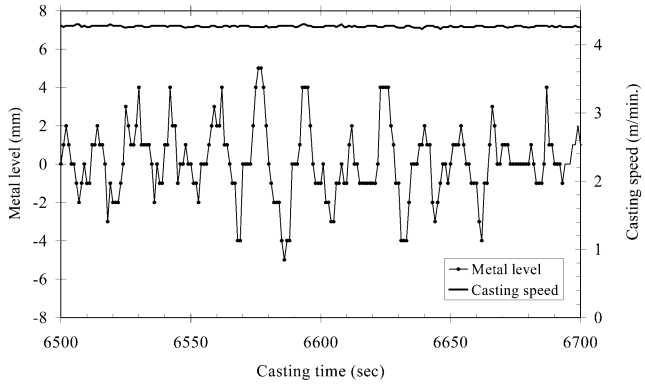

(*b*)

Fig. 2—The profiles of metal level and casting speed: (*a*) parallel mold and (*b*) funnel mold.

Hz, compared to the higher frequency of 0.3 Hz of the parallel mold. The detailed character of metal-level fluctuation, especially its effect on mold temperature, will be discussed in Part II in order to investigate its influence on mold crack formation.

The temperature of the inlet and outlet of the cooling water was measured in the parallel mold. Together with the water flow rate, this temperature difference (ΔT) was used to calculate the total heat removal rate. The ΔT stayed relatively constant during the entire heat (10 °C), although the inlet temperatures varied from 25 °C to 40 °C on the wide face of the mold.

Mold deformation during steady-state casting was measured at the junction between the wide and narrow faces of the parallel mold. During assembly, the wide face of the mold contacts continuously along the narrow-face edges. During operation, however, formation of a gap between these two faces above the meniscus has been reported.[2] This gap was measured using a simple metal-strip gauge during steady-state casting. After casting, the mold experiences permanent deformation due to residual inelastic strain.[2] Contraction of the mold width was measured at the top of the funnel mold using a ruler after 350 heats of casting.

Finally, a crack sample was obtained from a funnel mold after 345 heats of casting, and a metallurgical investigation was conducted. Details are presented in Part II together with a modeling investigation.

C. *Measured Mold Temperature Profiles*

The mold thermocouple-temperature data gathered during the plant trial were examined. Figure 3 shows the typical mold thermal response on the parallel mold for two thermocouples located at 176 mm below the top of the mold for an entire single-heat casting sequence. Both locations show similar amplitude of high-frequency thermal fluctuations (about 0.05 Hz). However, the thermocouple at the off-corner location, 376 mm from the mold center, is generally hotter than the other thermocouples. Moreover, the thermocouple located at the center of the mold exhibited significant variations of temperature over a long timescale (2000 to 5000 seconds), relative to other thermocouples. These long timescale variations have also been observed in conventional casting.[8–11] Figure 4 shows the thermal response at various distances below the mold top along the centerline of the parallel mold. It can be observed that, as expected, both the temperature and its fluctuation decrease with increasing

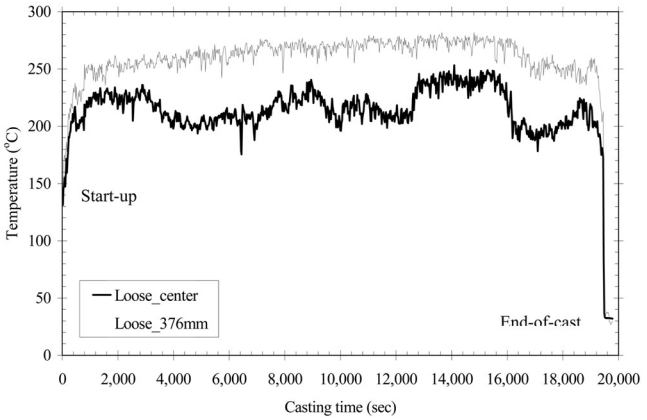

Fig. 3—Mold thermal response recorded at different mold locations around the mold perimeter at 176 mm below the top of the parallel mold (typical sequence).

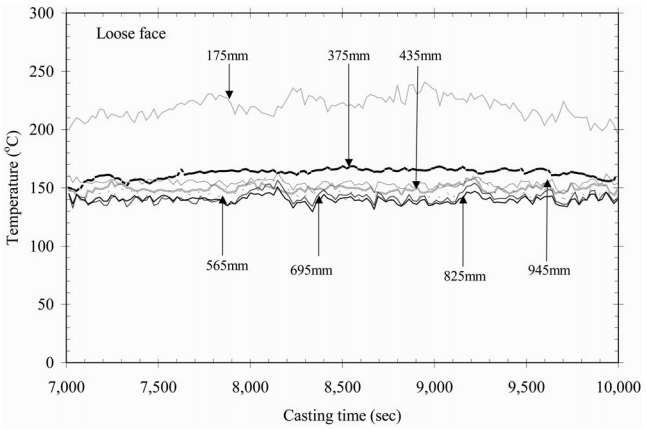

Fig. 4—Mold thermal response recorded at various axial locations down the centerline of the parallel mold during steady state.

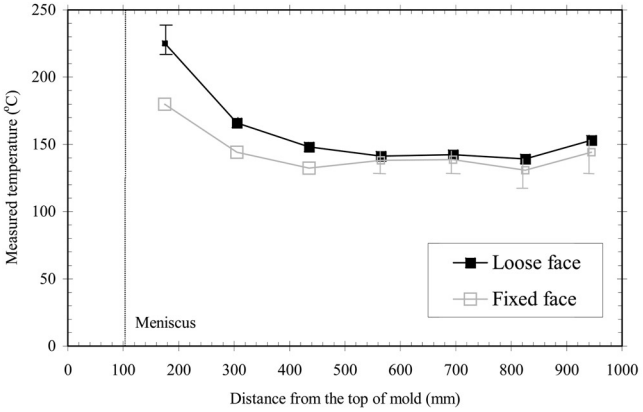

Fig. 5—Time-averaged temperature profile measured along the mold length (parallel mold).

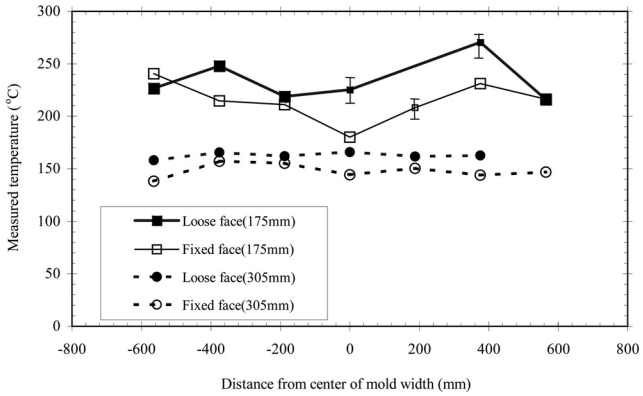

Fig. 6—Mold temperature profile measured at different positions across the wide face (parallel mold).

distance below the meniscus. Thus, at the lower part of the mold, the temperatures become close to each other.

To calculate the average temperature distribution in the mold wall and corresponding heat-flux profiles, mold temperature data obtained in the plant trial were averaged over 5 minutes of steady casting. Typical examples of the time-average measured mold temperature are presented in Figures 5 and 6. In these figure, the range of the data falls within the size of the symbols, except where noted with error bars. Figure 5 gives the temperature profiles along the centerline of the mold, which decrease with increasing distance from the meniscus as in conventional casting. As shown in this figure, the temperatures on the loose face (inner radius) are 10 °C to 50 °C higher than those of the fixed face, especially near the meniscus. The transverse temperature profiles across the broad face are plotted in Figure 6 at different distances below the top of the mold. The loose-face temperatures are consistently hotter than the fixed face regardless of position around the perimeter. Another striking feature is the deep valley in the temperature profiles in the central region of the wide face near the meniscus. Nonuniform temperature profiles across the mold width, especially around the meniscus, have been reported previously in both conventional slab casting[11,12,13] and thin-slab casting.[14]

D. *Discussion*

The variation of mold temperature around the submerged entry nozzle (SEN) may occur for numerous reasons. Factors, such as turbulence in the liquid slag pool and variations in slag flow into the strand-mold gap,[8] argon flow,[8] nozzle clogging,[9] SEN shape, and their associated effects on flow pattern of the molten steel[8–11] may contribute to the variation in the mold temperature. The trends in these measurements are generally consistent with previous measurements in conventional casters. Lower temperatures with greater variation near the meniscus at the central region of the mold width might be explained by several different phenomena. First, the high-speed steel flow pattern causes surface contour changes of the molten steel level at the meniscus, and associated variations in the mold-flux layer thickness across the width.[15] Birat *et al.*[16] measured the meniscus profile in a slab mold, which varied from −10 to 15 mm across the slab width with respect to the reference point. The meniscus shape also influences slag infiltration into the gap, which may affect significantly the mold temperature profile as well. Finally, the interaction between steel shell shrinkage and gap formation that is well-known in conventional casting[17] may cause local temperature drops or fluctuation in the funnel region. This awaits study in future research.

Table II. Simulation Conditions

(a) Mold Geometry	
Mold length (mm)	1000
Mold width (mm)	1660
Slab width (mm)	1260
Copper plate thickness (mm)	
Wide face	60 (parallel) 80 (funnel)
Narrow face	75
Water slot depth (mm)	35
Water slot thickness (mm)	5
Distance between slots (mm)	4.6
Nominal cooling water section (mm × mm)	5 × 10
Bolt length (mm)	445
Bolt diameter (mm)	16
Bolt hole diameter in water jacket (mm)	24
Distance between bolts (mm)	188
Water box thickness (mm)	360
Clamping force (kN)	
Top (0.58 m from bottom)	19
Bottom (0.1 m from bottom)	44
Tension bolt force	
Tightening torque, Nm	120
Friction coefficient	0.1

(b) Material Properties

	Copper (Plate)	Steel (Bolt)
Conductivity (W/mK)	350	49
Density (Kg/m^3)	8960	7860
Specific heat (J/KgK)	384	700
Elastic modulus (GPa)	115	200
Thermal expansion coefficient (1/K)	17.7×10^{-6}	11.7×10^{-6}
Poisson ratio	0.34	0.3

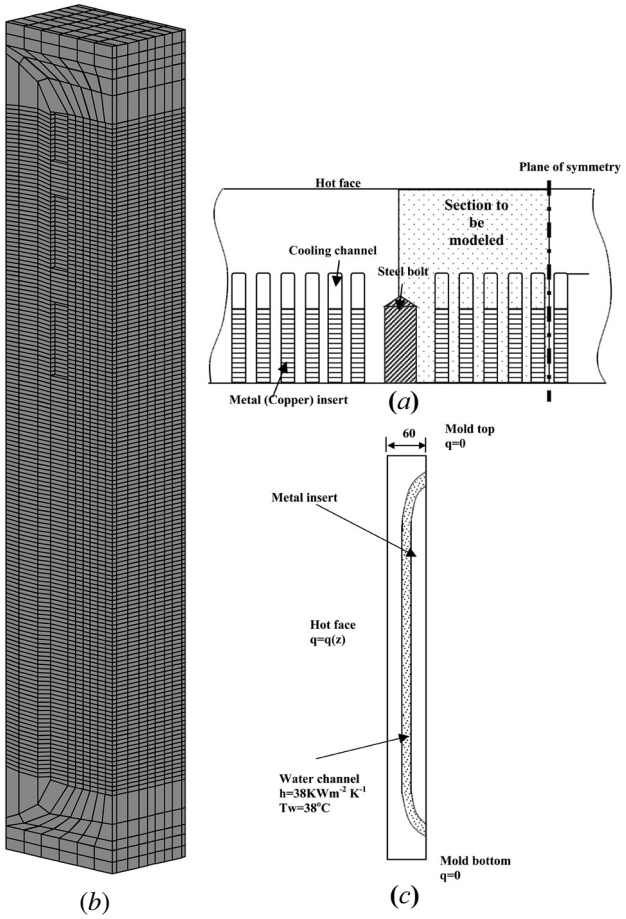

Fig. 7—The 2-D horizontal section through the wide face showing (*a*) top view of segment model domain, (*b*) corresponding 3-D section mesh, and (*c*) boundary conditions on a vertical section.

IV. THERMAL-STRESS COMPUTATIONAL MODEL DESCRIPTION

Finite-element models were developed to calculate temperature and the corresponding distorted shape of parallel and funnel molds during steady operating conditions and after cooling to ambient temperature using the commercial stress-analysis package, ABAQUS 5.8.[18] Model domains include typical two-dimensional horizontal sections through the copper plates, a 3-D segment model of a representative vertical segment of the mold, and a complete 3-D model of a one-quarter section of the mold, including the water jackets and bolts (3-D quarter model). Simulation conditions are given in Table II. Geometric domains are given in Figures 7 and 8, and properties are given in Table II and Figure 9.

A. *Heat Flow Model*

The heat flow model solves the transient heat-conduction equation[19] for the temperature distribution in the various model domains. Heat-flux data were input to the exposed surfaces of the copper elements on the mold hot faces as a function of position down the mold, as discussed later.

The 3-D segment model domain, shown in Figure 7, reproduces the complete geometric features of a typical repeating portion (Figure 7(a)) of the copper wide-face discretized into a fine mesh of 18,758 nodes and 14,622 eight-node brick elements.

A water-slot heat-transfer coefficient, h_1, was applied to the surface of the water slots and using the correlation of Dittus and Boelter,[20]

$$\frac{h_1 D}{k_w} = 0.023\left(\frac{DV_w\rho_w}{\mu_w}\right)^{0.8}\left(\frac{Cp_w\mu_w}{k_w}\right)^{0.4} \quad [1]$$

where, D is the hydraulic diameter of the slot, k_w is thermal conductivity, μ_w is viscosity, ρ_w is density, C_{pw} is the specific heat of the cooling water, and V_w is cooling-water velocity. For the cooling-water channel geometry and velocities in Tables I and II, these produce a heat-transfer coefficient of 38.45 kW/m^{2}K on the wide face and 36.17 kW/m^{2}K on the narrow face of the mold. Cooling-water temperatures were imposed as linear functions based on the inlet (top of the mold) and outlet (bottom of the mold) temperatures given in Table I. Heat-flux profiles are given in Figure 10 and were chosen to match the measured temperatures.

To simplify the geometry for the 3-D quarter-mold model, a pseudomodel was created using a coarse mesh of 759 nodes and 420 elements. The temperature field produced by the pseudomodel was arranged to match that of the 3-D segment model by artificially decreasing the water-slot heat-transfer coefficient and decreasing the hot-face heat-flux values. The accuracy of this approach was validated by comparing the results of this approach with the 3-D segment model. The maximum difference between them was 20 °C

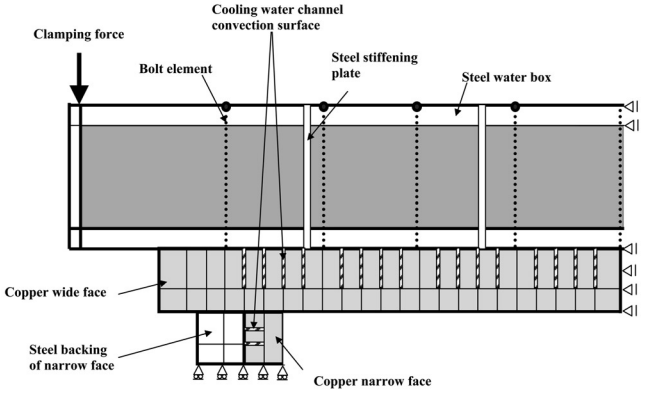

Fig. 8—Top view of 3-D quarter mold model showing boundary conditions.

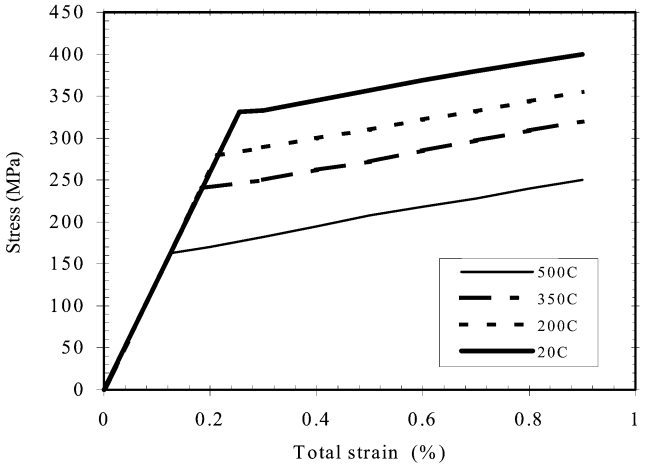

Fig. 9—Stress-strain curve for copper (Cr-Zr alloy) used in this model.[2]

on the hot face. To simulate thermal cycling of the mold over a complete campaign, it was assumed that the mold was heated from room temperature to the operating temperature by sudden immersion in the high-temperature environment for 100 seconds, followed by 4 hours of steady casting for each sequence, which includes five ladle changes. It was then cooled to room temperature, over 360 seconds after each sequence, which defines a single thermal cycle.

B. *Stress Model*

The thermal-stress model solves for the evolution of displacement and stresses in the mold during a 50-heat casting sequence, based on the previously calculated temperatures. Figure 8 shows the top view of the 3-D quarter-mold model used to analyze mold deformation. This model includes separate domains for the mold coppers and water jackets, which are coupled mathematically only at those points where they connect mechanically in the caster during operation. The cold side of the copper wide face is mathematically bolted to the back of the water jacket at 40 locations using two-node bar elements. Boundary conditions include clamping forces on the exterior of the water jacket (Table III) and a pretension force, F_{bolt}, in each bolt determined by the following equation:[2]

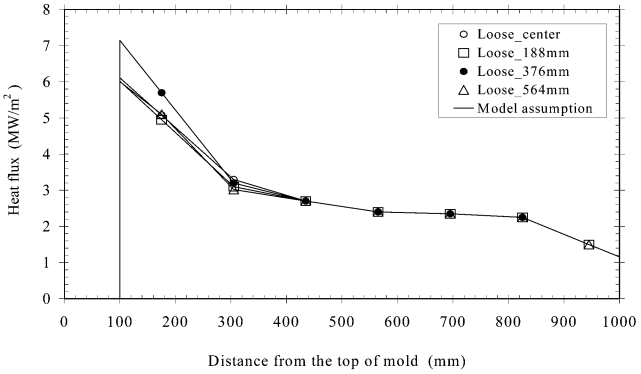

(*a*)

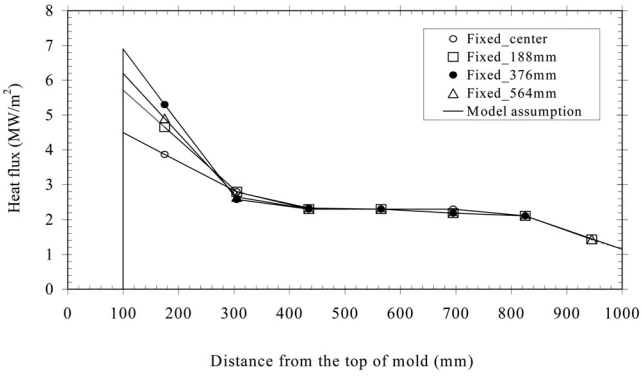

(*b*)

Fig. 10—Heat flux profiles of the parallel mold with different mold positions: (*a*) loose face and (*b*) fixed face.

$$F_{\text{bolt}} = \frac{2\tau}{d}\left(\frac{\pi d - \mu\lambda}{\lambda + \pi\mu d}\right) \qquad [2]$$

where τ is the bolt-tightening torque, d is the bold diameter, λ is the distance between threads of the bolt (1.5 mm), and μ is the friction coefficient, which varies from 0.2 (greased) to 0.6 (ungreased).

According to the preceding equation, the pretension force varies from 64.8 KN (greased) to 23.4 KN (ungreased). In the finite-element simulations, an average force between these two of 44 KN was chosen on each bolt.

Interface contact elements were used to prevent penetration between the contacting surfaces of the deforming wide and narrow faces of the mold and the water jacket. The maximum friction force between the faces, which depends on the normal pretension force (44 KN) from all of the bolts and the friction coefficient (0.6 maximum), is 1.02 MPa. This is negligible relative to the stresses generated by thermal expansion, which are on the order of the yield stress of 280 MPa at 350 °C. Thus, friction forces cannot prevent relatively free expansion of the copper plates, which agrees with findings for conventional molds.[2] In this study, a friction coefficient for relative sliding between contact surfaces of 0.1 was assumed to avoid convergence problems. This condition allows easy sliding, which is reasonable because the bolt holes are oversized and offer no resistance to sliding, as discussed in Part II. Finally, rigid body motion is prevented by constraining the symmetry planes from normal expansion and by fixing displacement at additional points.

This elastic-plastic-creep thermal stress model assumes

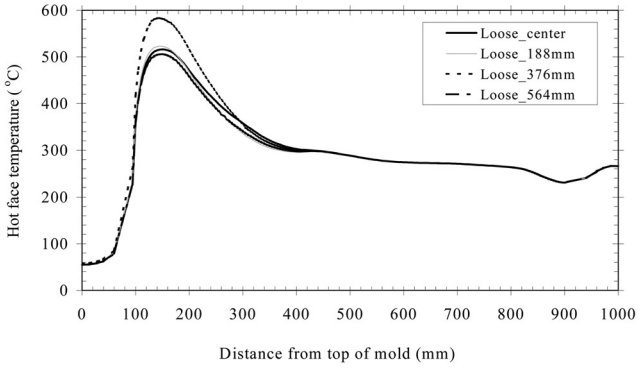

(*a*)

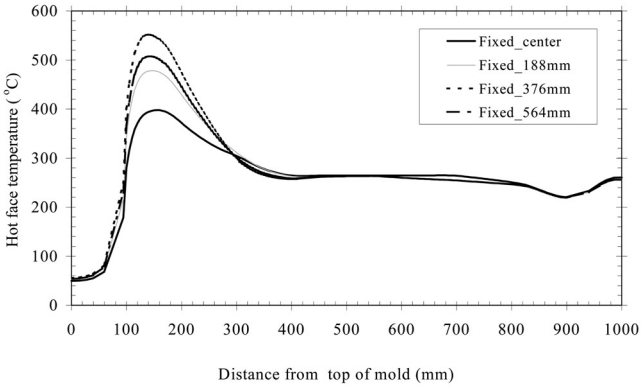

(*b*)

Fig. 11—Hot face temperature distribution down the length of the parallel mold: (*a*) loose face and (*b*) fixed face.

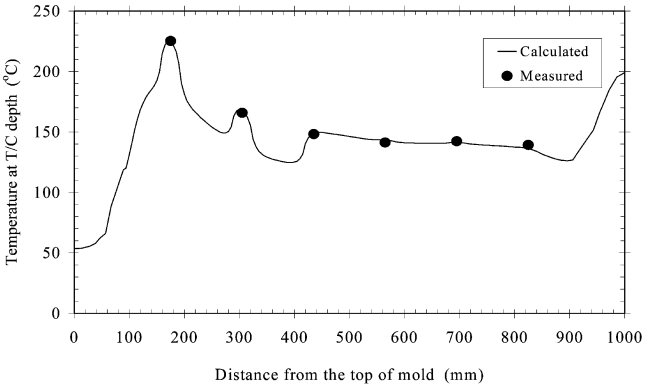

(*a*)

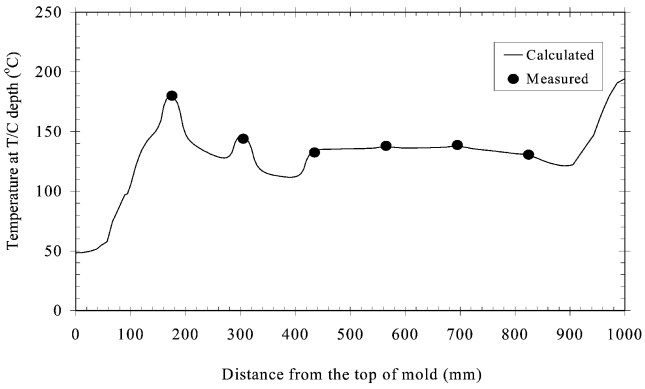

(*b*)

Fig. 12—Comparison of measured and calculated temperatures in the parallel mold: (*a*) loose face and (*b*) fixed face.

isotropic hardening with a temperature-dependent yield-stress function, shown in Figure 9. Considering that the total time of operation is less than 100 hours, primary creep is assumed, based on the following equation:[21]

$$\dot{\varepsilon}(\mathrm{s}^{-1}) = 2.48 \times 10^{14} \exp\left(\frac{-197{,}000}{8.31T(\mathrm{K})}\right) [\sigma(\mathrm{ksi}) - 23]^3 [t(\mathrm{s})]^{-0.92} \quad [3]$$

V. HEAT TRANSFER OF PARALLEL MOLD

A. *Heat-Flux Profiles*

To determine the heat-flux distribution on the 3-D mold faces, arbitrary heat-flux distributions were first applied as boundary conditions using the 3-D segment model described in Section IV. Then, these arbitrary values were adjusted until the temperatures calculated by the 3-D segment model at the thermocouple locations match well with the measured ones.

Figure 10 shows the heat-flux distribution over the wide face based on linear interpolation and extrapolation of the heat-flux values at the thermocouple positions. The peak values of heat flux at the meniscus were predicted to be about 7 MW/m^2, although they vary with mold position. These values are somewhat higher than other measurements reported for thin-slab casters, 5.5 MW/m^2.[7] There is uncertainty in the peak values extrapolated at the meniscus, however, because there are no thermocouples nearby.

B. *Hot-Face Temperature Profiles*

Axial mold-temperature profiles were calculated using the 3-D segment model based on the preceding heat-flux profiles given in Figure 10. Figure 11 shows the hot-face temperature distribution along the mold length at different positions across the wide face. As seen from this figure, the maximum temperature of the wide face is found about 20 mm below the meniscus and is 580 °C at the location of 376 m from the center of the mold. This is 200 °C higher than found in conventional slab casting owing to the higher casting speed. This is also 50 °C higher than previously reported for thin-slab casting.[7] These high temperatures may increase the possibility of mold crack occurrence, considering the softening temperature of Cu-Cr-Zr copper alloys of about 500 °C[22] It is important to note that within about 50 mm of the mold exit, the model predicts an increase in hot-face temperature of almost 50 °C. This surface is expected to be hotter, due to the end of the water slot, 28 mm above the mold exit.[2]

C. *Validation*

1. *Temperature profiles*

The degree of fit of the calculated heat-flux distribution is demonstrated by comparing the temperatures measured by the thermocouples in the mold wall with the calculations based on the heat-flux profiles in Figure 10. Figure 12 shows complete temperature profiles along the midplane of this parallel mold at the depth below the hot face where the

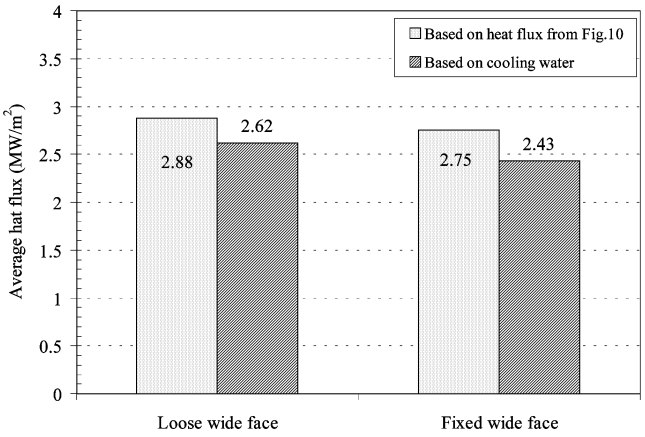

Fig. 13—Comparison of average heat flux calculated from heat flux data and from energy balance on cooling water.

thermocouples are located. The dips are caused by the extra-angled water slots (Figure 1), which provide extra cooling to the region near the meniscus, except for near the bolt holes, which contain the thermocouples. The temperature increase of 75 °C near the mold bottom is caused by the extra distance of the hot face from the cooling water after the water slots end. As can be seen from this figure, although there is some difference between measured and calculated values, on the whole, the model predictions agree reasonably well with the measured temperatures. This comparison confirms that the heat-flux curves in Figure 10 are calibrated properly.

2. *Heat-flux profiles*

To validate the heat-flux profiles, energy balances were performed on the cooling water for each face of the mold. During the process of cooling the mold, the water heats up; and this temperature difference (ΔT) between the inlet and outlet of the cooling water is commonly used to monitor the total heat-removal rate of the mold. Multiplying the temperature rise for each face by the corresponding water flow rate gives the total rate of heat removal from that face. Dividing this by the exposed mold face area gives an average heat flux extracted by that face. These measured values are compared in Figure 13 with the total calculated heat fluxes (area under Figures 10(a) and (b)). Although there is some mismatch, considering the experimental uncertainties, the variation of measured temperatures and the uncertainty of the heat-flux value extrapolated at the meniscus, the heat-flux distribution down the mold length appears to be reasonable.

VI. THERMAL AND MECHANICAL BEHAVIOR OF PARALLEL MOLD

A. *Results*

The typical temperature and distorted shape of the parallel quarter mold during operation are shown in Figures 14 and 15 for conditions in Table II. Figure 14 shows the mesh, temperature contours on the hot face, and the distorted shape of the mold, exaggerated fifty-fold. At the hot face, the maximum temperature is found to occur approximately 370 mm from the centerline.

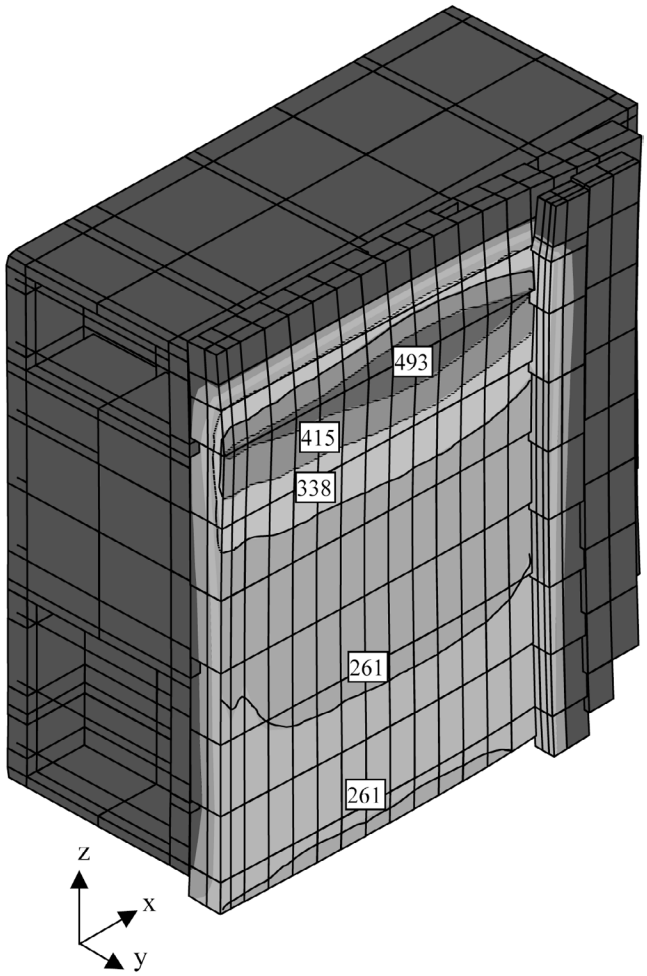

Fig. 14—Temperature contours on distorted mold shape during operation for the parallel mold.

The results shown in Figures 14 and 15 provide insight into the mechanical behavior of the mold during operation. The copper hot face expands in proportion to its temperature increase but is restrained by the cold copper beneath it. Consequently, the copper plates bend outward toward the molten steel in a manner similar to the conventional slab mold.[2] The peak distortion of 0.3 mm, which occurs below the meniscus along the center of the wide face, is smaller than that of a conventional caster predicted by Thomas *et al.*,[2] even though the heat flux is higher for thin-slab casting. This is because the water box is 360-mm thick, which is thicker than conventional slab molds. As explained by Thomas *et al.*, water box rigidity is more important to distortion than hot-face temperature.

The bending of each copper plate toward the liquid steel stretches the bolts and pulls it away from the front of the water jacket during operation. Despite the bolt prestress of 44 KN, a thin gap forms just below the meniscus, as shown in Figure 15. The gap between the water box and the copper cold face is 0.2 mm in a 60-mm thickness of parallel mold, where distortion is greatest. Figure 16 shows the evolution of thermal behavior during the first heat and subsequent cooling. The reversal in curvature is similar to that of conventional slab molds.[1,2]

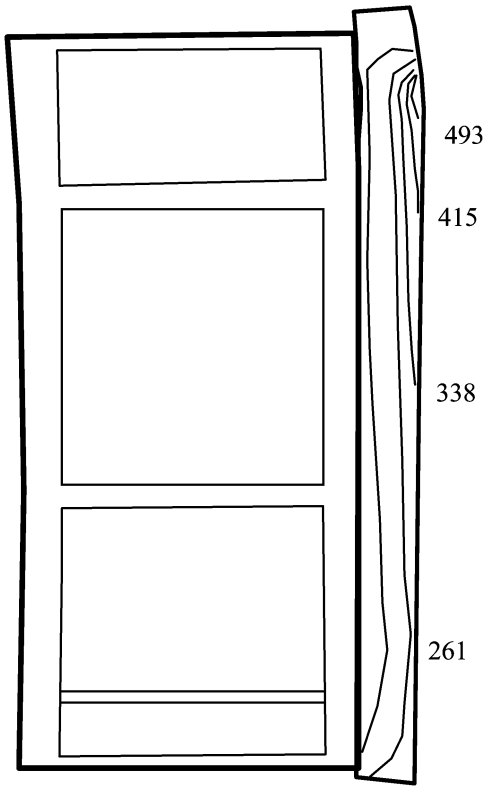

Fig. 15—End view of distorted mold along the wide face centerline showing the gap between copper plate and water jacket and temperature profiles.

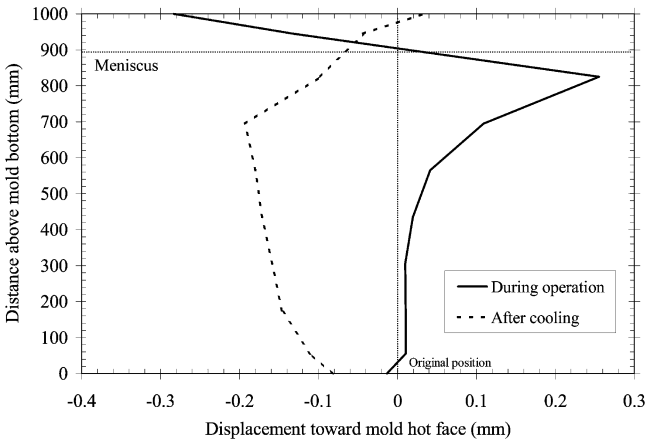

Fig. 16—Predicted evolution of thermal distortion on vertical section for the parallel mold (centerline surface).

B. *Validation*

To validate the stress model predictions, comparisons were made with plant trial measurements on the parallel mold. Figure 17 compares measured and predicted distortion of the wide and narrow faces along their line of intersection. The gap measured with a simple metal-strip gauge at the junction between the wide and narrow face was 0.35 mm. Although the calculated value is about 30 pct larger than the measured value, this general agreement suggests an accurate prediction of mold behavior. If larger, this gap between the plates above the meniscus may cause problems since the

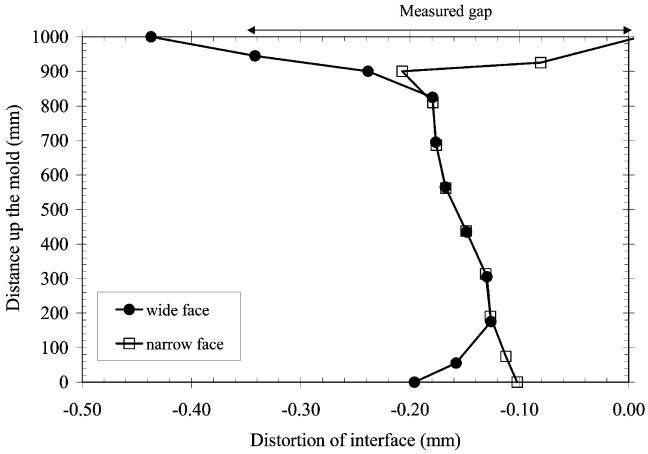

Fig. 17—Distortion of wide and narrow faces along the line where they meet in the parallel mold.

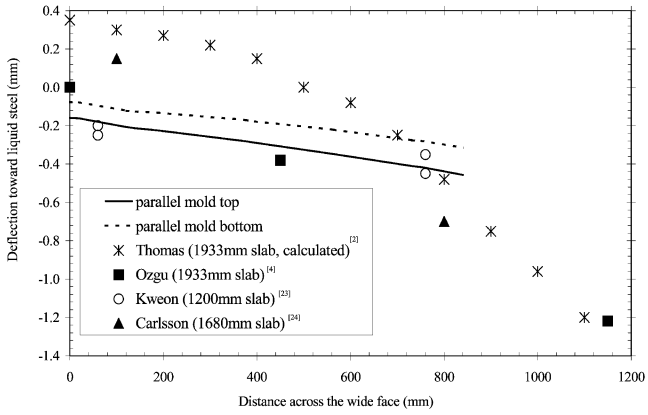

Fig. 18—The behavior of back plate distortion for the parallel mold during operation (relative to zero along centerline through narrow faces).

mold flux might penetrate, freeze, and aggravate mold wear and shell sticking at this critical junction.[2]

Figure 18 compares the calculated backing-plate distortion with measurements from several conventional casting molds.[4,23,24] The predicted trend is consistent with both the measurements and previous calculations.[2] The distortion depends on hot-face temperature and water box rigidity[2] and is influenced greatly by the casting speed, mold construction, slab width, and other parameters, so a quantitative match is not expected.

Permanent mold-width contraction was also reported after casting.[2] Figure 19 shows the calculated evolution of total contraction of the mold width at the top of the funnel mold during a typical campaign of 70 casting sequences. Each sequence is assumed to include five heats (average) or 4 hours, which involves a single thermal cycle of filling and emptying the mold. This is compared with the measured width contraction after 350 heats and with computations by Hashimoto *et al.*[6] for a conventional mold. As can be seen in this figure, most of the permanent deformation occurs during the first thermal cycles (sequences). It also reveals a very small but roughly constant decrease in width for each subsequent sequence, leading to a total width contraction of about 0.7 mm (0.042 pct of residual inelastic strain) after

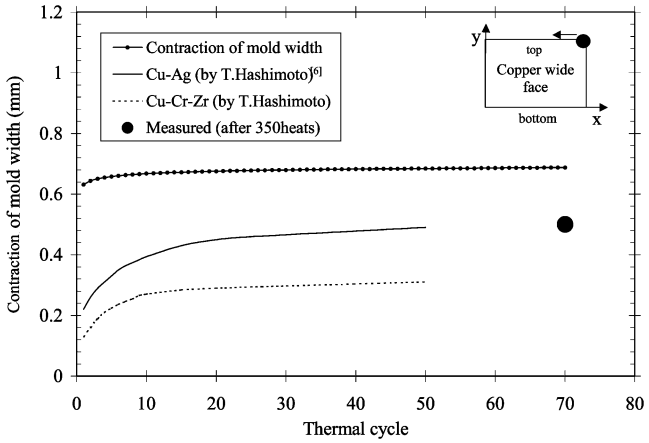

Fig. 19—Comparison of calculated and measured total mold width contractions during a typical casting campaign for the funnel mold.

the campaign. This is comparable to the measured value of 0.5 mm. Both the measured and calculated values are comparable to the prediction of permanent mold-width contraction by Hashimoto *et al.*[6] and Thomas *et al.*,[2] who predicted that permanent contraction varies from 0.02 to 0.08 pct, depending on the constraint of mold. The small contraction for the high-temperature mold in this work is due to the lack of constraint offered by the oversized bolt holes in this mold (Part II).

VII. COMPARISON OF PARALLEL AND FUNNEL MOLD

Next, a study was undertaken to compare the thermomechanical behavior of parallel and funnel molds using the quarter-mold model. To enable a comparison isolating the effect of geometry alone, heat flux, q, in both molds was defined by the following equation:[25]

$$q(KW/m^2) = 5403 - 990\sqrt{t(\text{sec})} \qquad [4]$$

Figure 20 shows the temperature and thermal deflection of the wide face during operation for this heat-flux profile for the different mold shapes. The figure also shows the differences that arise between temperature predictions of the course-mesh 3-D quarter-mold model and the 3-D segment model if the heat-flux conditions are not adjusted.

As can be seen from Figure 20(b), the deflection behavior for the parallel mold does not change much with position across the mold width. However, the funnel mold deflection varies considerably with position. Specifically, the center of the mold width corresponding to the funnel region has less deflection, while the edge region of the funnel has more deflection, relative to the parallel mold. These phenomena can also be observed when distortion of the hot face is plotted across the mold width at the 75-mm position below the meniscus in Figure 21.

The maximum deflection in both molds is relatively small (<0.3 mm). The effect of mold-plate thickness on mold distortion is due mainly to the effect of effective plate thickness on the hot-face temperature.[2] These different behaviors of distortion can be explained by the difference of mold shape on plate thickness. In the parallel mold, the plate thickness is constant. However, the funnel mold plate has a

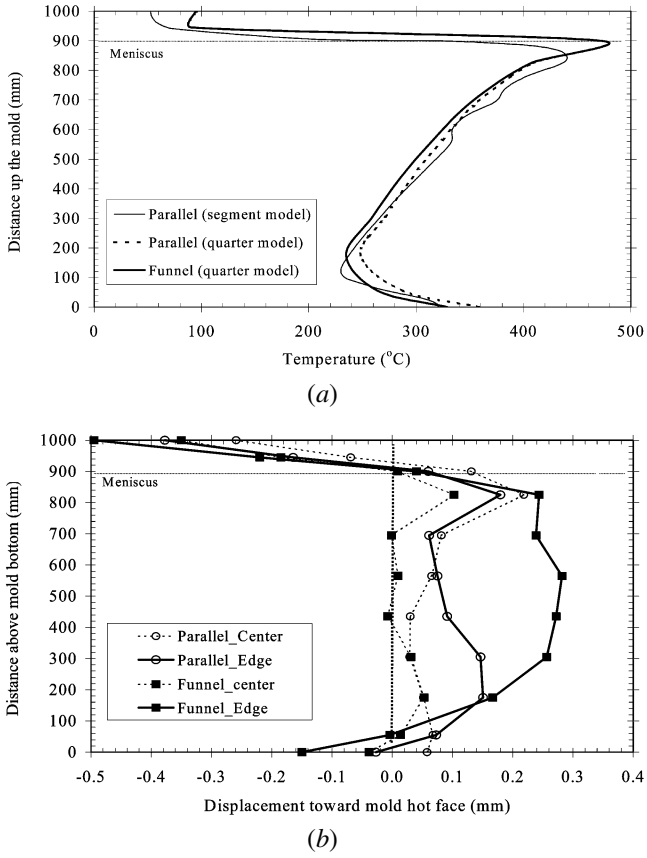

Fig. 20—Comparison of thermal mechanical behavior of parallel and funnel molds during operation: (*a*) hot face temperature profile and (*b*) distortion along different vertical sections.

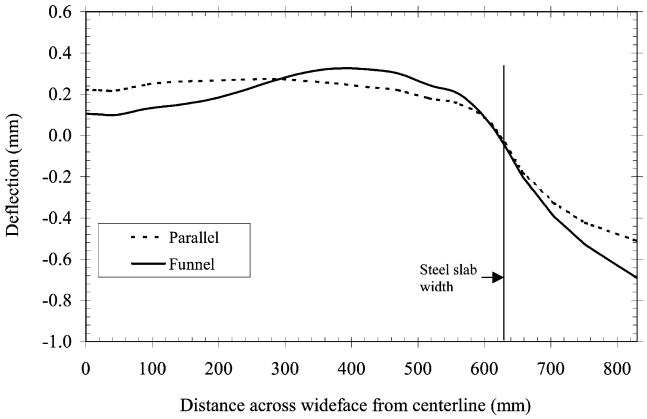

Fig. 21—Mold distortion of parallel and funnel molds across the wide face at 175 mm below the mold top during operation.

variable thickness across the mold width. Specifically, at the center of the funnel mold, the plate thickness is less than that of the parallel mold. It gradually becomes thicker, and, at the edges of the funnel mold, the plate thickness is larger than that of the parallel mold. Although the effective mold-wall thickness (distance between the cooling channel and the hot face) is the same for both molds, the plate thickness still has a small effect on distortion. Specifically, the regions with a thick plate have slightly more distortion (for the same hot-face temperature). This agrees with the results of Thomas *et al.*[2]

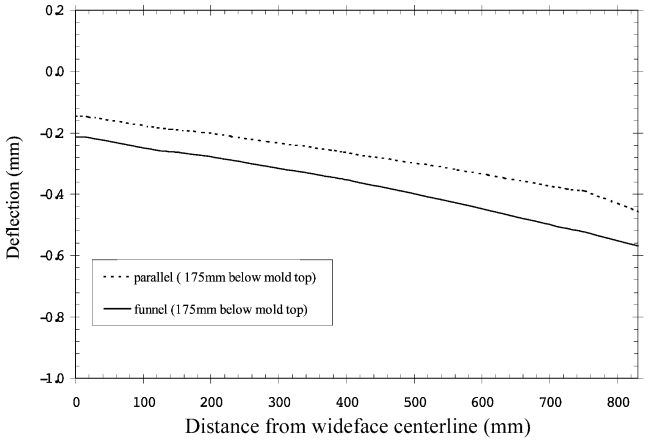

Fig. 22—The behavior of back plate distortion during operation according to the mold shape.

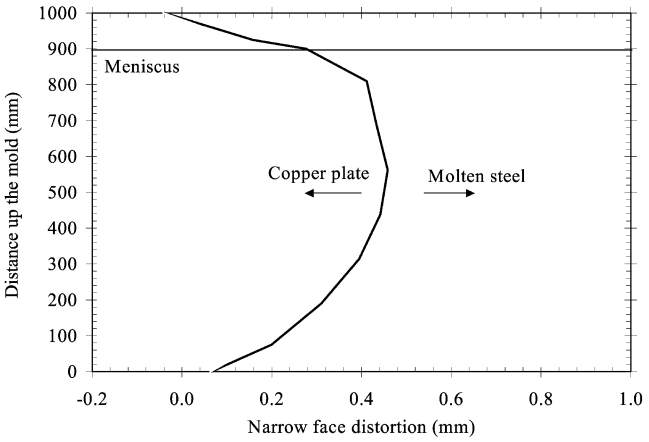

Fig. 23—Predicted distortion profile down the narrow face of the parallel mold.

Figure 22 shows the deflection of the backing plate relative to its original position along the wide face. Distortion of the backing plate for the funnel mold is slightly larger than that for the parallel mold due to its larger plate thickness at the corner (junction with narrow face).

When casting a slab, gaps between the shell and mold tend to form near the narrow face of the mold because of shrinkage of the solidifying shell on the wide face. The size of the gap is controlled by imposing taper along the mold walls. In addition to the shrinkage, it is also important to know how the mold distorts because this contributes to the mold taper. Figure 23 shows the displacement of the narrow face of the mold, which is qualitatively similar to the wide face. This behavior is affected mainly by the rigidity of the narrow-face backing plate. Any differences between the behavior of the funnel and parallel molds should be due to differences in the narrow-face backing plate, which were not studied.

VIII. CONCLUSIONS

The thermal and mechanical behavior of a thin-slab mold has been investigated using measurements conducted on an operating caster at POSCO and a 3-D heat transfer and thermalelastic creep model with ABAQUS.

1. The model predictions of temperature and distortion during operation match plant observations.
2. Heat-flux profiles, based on measured temperatures for 3.6 m/min casting speed, show that thin-slab casters have much higher heat extraction than conventional casters, ranging from 2.4 to 2.6 MW/m^2, with peak meniscus heat flux approaching 7 MW/m^2.
3. During operation, the hot-face temperature reaches 580 °C and is highest 20 mm below the meniscus towards the mold edges 370 mm from the centerline.
4. The copper plates bend toward the steel as in a conventional caster with a maximum distortion toward the liquid steel of only 0.3 mm. This occurs just above the center of the wide faces and is generally less than the distortion of a conventional mold, owing to the increased thickness and corresponding rigidity of the water box.
5. Residual distortion is smaller than previous measurements, owing to oversized bolt holes in the water box, which do not over constrain the thermal expansion and contraction.
6. The thickness variations of the funnel mold lead to a different shape-distortion profile than in a parallel mold. The distortion magnitudes are quite similar, however, with maximum values of 0.25 mm (funnel) and 0.22 mm (parallel mold).

ACKNOWLEDGMENTS

The authors thank POSCO for permission to publish this article. The authors are indebted to many people in the Technical Research Lab., POSCO. In particular, we acknowledge the support of Dr. S.Y. Kim, who supplied plant trial measurement data, and Mr. W.W. Hur and Dr. C.H. Yim, for their cooperation and assistance. The authors are also grateful for helpful discussions with Dr. T.J. Yeo and Mr. J. Shaver. Support of BGT from the Continuous Casting Consortium at the University of Illinois and from the National Science Foundation (Grant No. DMI 98-00274) is also acknowledged. Funding for this project from POSCO is gratefully acknowledged.

REFERENCES

1. B.G. Thomas, G. Li, A. Moitra, D. Habing, and J. Azzi: *Proc. 1st Eur. Conf. Casting*, 1991, vol. 2, pp. 417-26.
2. B.G. Thomas, G. Li, A. Moitra, and D. Habing: *Iron Steelmaker*, 1998, vol. 25 (10), pp. 125-43.
3. K. Tada, S. Kasai, A. Ichihara, and H. Onishi: *Kawasaki Steel Tech. Rep. 4*, 1987, vol. 17, pp. 26-33.
4. M.R. Ozgu: *Can. Metall. Q.*, 1996, vol. 35 (3), pp. 199-223.
5. D.M. Salkiewicz and J.O. Ratka: *78th Steelmaking Conf. Proc.*, ISS-AIME, Warrendale, PA, 1995, vol. 78, pp. 369-76.
6. T. Hashimoto, K. Ohnishi, M. Yamaguchi, M. Kinugawa, and M. Ueda: *Hitachi Zosen Tech. Rev.*, 1982, vol. 43, pp. 1-9.
7. T.G. O'Connor and J.A. Dantzig: *Metall. Mater. Trans. B*, 1994, vol. 25B, pp. 443-57.
8. S.G. Thornton and N.S. Hunter: *73th Steelmaking Conf. Proc.*, ISS-AIME, Warrendale, PA, 1990, vol. 73, pp. 261-74.
9. W. Lai, M. Milone and I.V. Samarasekera: *83rd Steelmaking Conf. Proc.*, ISS-AIME, Warrendale, PA, 2000, vol. 83, pp. 261-74.

10. M.R. Ozgu and B. Kocatulum: *76th Steelmaking Conf. Proc.*, ISS-AIME, Warrendale, PA, 1993, vol. 76, pp. 261-74.
11. S.L. Kang, I.J. Lee, S.D. Shin, S.M. Yang, H.B. Lee, J. Choi, and I.R. Lee: *77th Steelmaking Conf. Proc.*, ISS-AIME, Warrendale, PA, 1994, vol. 77, pp. 347-56.
12. R.J. O'Malley: *82nd Steelmaking Conf. Proc.*, ISS-AIME, Warrendale, PA, 1999, vol. 82, pp. 13-33.
13. H.L. Gilles: *76th Steelmaking Conf. Proc.*, ISS-AIME, Warrendale, PA, 1993, vol. 76, pp. 315-29.
14. K. Wunnenberg and K. Schwerdtfeger: *Iron Steelmaker*, 1995, vol. 22 (4), pp. 25-31.
15. B.G. Thomas, A. Morita, and R. McDavid: *Metal. Mater. Trans. B*, 1996, vol. 27B, pp. 672-93.
16. J.P. Birat, M. Larreq, J.Y. Lamant, and J. Petegnief: *74th Steelmaking Conf. Proc.*, ISS-AIME, Warrendale, PA, 1991, vol. 74, pp. 315-29.
17. A. Moitra, B.G. Thomas, and H. Zhu: *76th Steelmaking Conf. Proc.*, ISS-AIME, Warrendale, PA, 1993, vol. 76, pp. 657-67.
18. *ABAQUS*, Hibbitt, Karlsson & Sorensen, Providence, RI, 1996.
19. I.V. Samarasekera and J.K. Brimacombe: *Ironmaking and Steelmaking*, 1982, vol. 9 (1), pp. 1-15.
20. F.P. Incropera and D.P. Dewitt: *Fundamentals of Heat Transfer*, J. Wiley & Sons, New York, NY, 1981, p. 401.
21. G. Li, B.G. Thomas, and J.F. Stubbins: *Metall. Mater. Trans. A*, 2000, vol. 31A, pp. 2491-502.
22. Kabelmetal: *Technical Information 0805*, Germany, 1997.
23. O.D. Kweon: POSCO, Pohang, Korea, personal communication.
24. G. Carlsson, B. Brolund, and R. Nystrom: *Journees Siderurgiques ATS*, Paris, Dec. 6–7, 1989.
25. J.K. Park, B.G. Thomas, and I.V. Samarasekera: *83rd Steelmaking Conf. Proc.*, ISS-AIME, Warrendale, PA, 2000, vol. 83, pp. 9-21.

Summary of Comments on METB02C271

Page: 2

Sequence number: 1
Author: IPC
Date: 3/4/2002 12:20:06 PM -24'00'
Type: Note
Au: Table I: Column head for column 1?

Page: 5

Sequence number: 1
Author: IPC
Date: 3/4/2002 12:20:30 PM -24'00'
Type: Note
Au: Vendor name and location?

Sequence number: 2
Author: IPC
Date: 3/4/2002 12:21:00 PM -24'00'
Type: Note
Au: Which particular section?

Page: 6

Sequence number: 1
Author: IPC
Date: 3/4/2002 12:21:23 PM -24'00'
Type: Note
Au: There is no Table III. Please advise.

Page: 12

Sequence number: 1
Author: IPC
Date: 3/4/2002 12:22:18 PM -24'00'
Type: Note
Au: Reference 22: City location? Is the data set accurately?

Sequence number: 2
Author: IPC
Date: 3/4/2002 12:22:17 PM -24'00'
Type: Note
Au: Reference 23: Year?

Online Proofing Guidance Page

FIRST STEP:

Install Adobe Acrobat Reader if you do not already have this or another Acrobat product installed on your computer. You can do this free of charge by connecting to the Adobe site and following the instructions at:

http://www.adobe.com/products/acrobat/readermain.html

SECOND STEP:

Please download and print your PDF file — we recommend that you save this file to disk, rather than opening it from within your Browser.

From a PC:

1. Right-click on the file/article link.
2. Select ''Save Target as''
3. Select a desired location on your computer to save the file to, and click on ''Save''
4. Open your PDf file directly with Acrobat Reader or another Acrobat product.
5. Print this file as you normally would with any typical application. Example: Go up to your toolbar, select ''File'', select ''Print''.

From a MAC:

1. Hold the mouse button down over the link.
   a. In Internet Explorer, select ''Download Link to Disk'' from the resulting pop-up menu
   b. In Netscape, select ''Save this Link as'' from the resulting pop-up menu
2. Select a desired location on your computer and click on ''Save''
3. Open your PDF file directly with Acrobat Reader or another Acrobat product.
4. Print this file as you normally would with any typical application. Example: Go up to your menu bar, select ''File'', select ''Print''.

THIRD STEP:

Please go through the file you have just printed and thoroughly and clearly mark any revisions you would like to see implemented in your paper. If you have had any changes in phone/fax or e-mail addresses since your paper was submitted, please send us this new information.

FOURTH STEP:

Your revised paper needs to be faxed or mailed to:

IPC Communication Services
Attn: Sheryl Dickenson
501 Colonial Drive
St. Joseph, MI 49085
Fax number: 1-616-983-4064

If you have questions regarding your paper in general, you may email or telephone:

IPC Communication Services
Attn: Sheryl Dickenson
Email: sdickens@ipcjci.com
Phone: 1-616-983-7412, ext. 529